Transient Electric Field Shaping With the Linear Combination of Configuration Field Method for Enhanced Spatial Control of Microwave Plasmas

Valentin Mazieres, Ali Al Ibrahim, Cedric Chauviere, Pierre Bonnet, Romain Pascaud, Richard Clergereaux, Simon Dap, Laurent Liard, Olivier Pascal

Date of publication xxxx 00, 0000, date of current version 05/06/2020.

Digital Object Identifier 10.1109/ACCESS.2017.DOI

Transient Electric Field Shaping With the Linear Combination of Configuration Field Method for Enhanced Spatial Control of Microwave Plasmas

V. Mazières[1,2], A. Al Ibrahim[3], C. Chauvière[4], P. Bonnet[3], R. Pascaud[2], R. Clergereaux[1], S. Dap[1], L. Liard[1], and O. Pascal[1].

[1]Laboratoire LAPLACE, Université Paul Sabatier, 118 route de Narbonne, 31062 Toulouse, France
[2]ISAE-SUPAERO, Université de Toulouse, 10 avenue Edouard Belin, 31055 Toulouse France
[3]Université Clermont Auvergne, CNRS, SIGMA Clermont, Institut Pascal, F-63000 Clermont-Ferrand, France
[4]CNRS, UMR 6620, Laboratoire de Mathématiques, F-63171 Clermont-Ferrand, France

Corresponding author: V. Mazières (e-mail: valentin.mazieres@laplace.univ-tlse.fr).

The authors want to acknowledge the DGA/AID for their funding support and the CEA-Gramat for the material support.

ABSTRACT The demonstration of enhanced spatial control of nanosecond microwave plasmas generated by the time reversal plasma source is presented in this paper. This new microwave plasma source relies on the spatio-temporal control of the electric field inside an all-metal plasma reactor by modifying the waveform of a high power microwave signal. More specifically, it originally used the spatio-temporal focusing capabilities of the time reversal method to focus a high electric field in a small location. However, a parasitic microwave breakdown can still occur at sharp corners or wedges inside the cavity due to the local enhancement of the residual electric field during time reversal focusing. Thus, it is proposed to use the linear combination of configuration field method to improve field control inside the reactor. Its transient electric field shaping capabilities turn out to be a good candidate for the development of a low pressure microwave "plasma brush".

INDEX TERMS Microwave plasma sources, Transient field shaping, Inverse source problem, Reverberation chamber, Time reversal.

I. INTRODUCTION

Low pressure microwave plasmas are widely used for various processes such as cleaning, activation, etching, or coating [1]–[3]. Microwave sources allow for very efficient generation of isotropic plasmas without electrodes that could lead to its contamination.

A microwave plasma source often consists of a continuous wave (CW) power source at 915 or 2450 MHz, a microwave-to-plasma applicator, and a plasma vessel [1]. It may be combined with a static magnetic field as in electron cyclotron resonance (ECR) excited plasma that exhibits better uniformity and higher plasma densities [4]. The microwave-to-plasma applicator is usually designed together with the plasma vessel to optimize the spatial distribution of the electric field which is responsible for plasma breakdown and sustainment. As a result, many microwave plasma sources can be found in the literature [5].

The travelling-wave-sustained microwave discharges, for example, are made up of a glass tube inserted into a microwave-to-plasma applicator, also known as surface-wave launcher [6]. Several types of surface-wave launchers have been proposed such as the Surfatron [7], composed of coaxial transmission line elements, and a surfaguide [8], a device based on rectangular waveguides. Here, the plasma is produced by a propagating surface-wave along the plasma in the glass tube, while the surface-wave propagation is sustained by the plasma itself. Large-area microwave plasmas can also be generated by radiating microwave power with a slot antenna array [9], [10]. The microwave-to-plasma applicator, called the slot antenna array, can have a linear, rectangular, circular, or annular geometry depending on the plasma vessel. Another common way to produce microwave plasmas is to increase the intensity of the electric field in a closed metallic cavity that acts as the plasma vessel by using its resonance modes [11]–[13]. Such plasma reactors are

widely used for diamond synthesis using plasma-enhanced chemical vapor deposition [14]. Their design is based on the optimization of the cavity geometry to shape the electric field inside. Thus, the reactor can take a cylindrical [15], ellipsoidal [16], or even more complex shapes [17].

These microwave plasma sources primarily allow the generation of large, dense, and uniform plasmas. Another common point between these sources is that once their design is complete, the location of the plasma in the vessel is fixed once and for all.

Recently, Mazières *et al.* proposed to develop a new kind of microwave plasma source: "the plasma brush" [18]. As opposed to the sources mentioned above, the idea is not to create a plasma occupying the entire volume of a large plasma vessel, but rather to generate a localized plasma whose position is controlled in real time for local material processing of large objects. Practical implementation thus requires the generation and control of arbitrarily shaped electromagnetic fields in the plasma vessel. In [18], this source was demonstrated experimentally for the first time using the time reversal (TR) method.

The spatial and temporal focusing properties of TR were demonstrated for microwave applications by Lerosey *et al.* [19]. They have since been applied for wireless communications [20], [21], source localization [22], and wireless power transfer [23], [24]. In a TR experiment, the field radiated by a source is first recorded using an array of antennas known as the time reversal mirror (TRM) [25]. The recorded signals are then time reversed and retransmitted by the same TRM, leading to spatio-temporal focusing of the waves at the initial source. In a complex reverberating propagation environment such as our electrically large all-metal plasma vessel, it is possible to highly reduce the complexity of the TR system by considering only one element for the TRM and taking advantage of multipath [19], [26]. This property was actually used in the demonstration reported in [18].

As TR is a transient electric field shaping method, it has several differences with common microwave plasma sources. Thus, the plasma location is controlled by modifying the waveform transmitted into the cavity, which results in broadband rather than monochromatic microwave signals. Moreover, temporal focusing of TR leads to nanosecond microwave pulses instead of CW microwave power at the plasma location. However, it has been shown that it is still possible to generate and sustain plasma discharge using repetitive nanosecond microwave pulses [18].

Despite its obvious focusing capabilities, the original TR method still has some limitations for the spatial control of microwave plasmas. As shown in this paper, further undesired plasmas may appear in the cavity. These parasitic discharges are produced where the electric field is enhanced by the geometry of the elements inside the cavity such as the corners and wedges of the sample holder or the object to be processed [27] or the presence of screws, defects, gaps, or metallic grids [28], [29]. These parasitic discharges result from the residual spatial sidelobes during TR focusing. These spatial sidelobes are evaluated by measuring the spatial peak-to-noise ratio which is the ratio between the magnitude of the refocusing peak, at the position and moment of the peak, and the magnitude of the lobes all around the cavity. This ratio is governed by the modal regime, namely undermoded or overmoded, and the degree of chaoticity of the cavity [30], [31]. In order to improve the spatial control of microwave plasmas, one can therefore work on the cavity design [32].

Another approach is to consider transient electric field shaping methods that constrain the electric field magnitude at several locations over time. This requires solving inverse source problems in order to determine the temporal source that leads to the desired behaviour of the electromagnetic field. The focusing properties of TR and its adaptability to the propagation environment have encouraged the development of new TR-based methods, such as generalized TR which can be used to generate coherent wavefronts within complex media [33] or other techniques that generate microwave spatial fields with arbitrary patterns [34], [35], even at subwavelength scale [36]. Indeed, by knowing the impulse response between two points in a complex medium, TR can focus waves at one of these points at a given time. Using a set of several points, the superposition principle then allows complex spatially inhomogeneous field distribution to be shaped at the focusing instant [34]–[36]. TR has also been used for nulling the field at a given position and time [37], even with simultaneous focusing at another location using several antennas in the TRM [38].

However, none of these methods can be used to avoid the generation of parasitic discharges because it is necessary to control electric field distribution during the whole experiment and not just at a given time. Other time-domain methods have been developed to shape electromagnetic fields mainly based on the Hilbert Uniqueness Method (HUM). Nevertheless, the authors in [39] indicated that HUM suffers from intrinsic limitations during experiments such as requirement of prior knowledge of the transient noise in the system. The robustness of the HUM approach with respect to time and the discretized geometry is still under study. Consequently, Spirlet *et al.* developed an alternative frequency-domain technique based upon the optimal control theory of partial differential equations to shape time-harmonic electromagnetic waves [40]. The mathematical theory behind the developed method is complex and requires accurate modeling of the experimental setup. Here, we present an alternative solution which does not have such drawbacks. Recently, Benoit *et al.* introduced a simple and efficient method called the linear combination of configuration field (LCCF) to determine a temporal source that leads to predefined electromagnetic fields at one or more positions over a given interval of time [41]. First, as for a TR experiment, the impulse responses are recorded between the source point and the receiver points. Then, the LCCF finds a linear combination of these responses to compute the desired source. Emission of this source yields

the desired target electromagnetic fields, and this for an arbitrary duration [42].

In this paper, we propose to use the LCCF method to enhance the spatial control of microwave plasmas. Section II presents the proposed microwave plasma source. In Section III, we discuss the limitations of the original TR method for our application. The LCCF method is then presented in Section IV-A. Finally, Section IV-B shows the experimental results and the enhanced control obtained by the LCCF method.

II. EXPERIMENTAL SETUP

Our experimental setup presented in Fig. 1 is similar to the setup previously used in [18]. The experiments take place in a plasma reactor, namely a reverberant metallic cavity, of dimensions 0.6 m $\times$ 0.6 m $\times$ 0.3 m, that is to say $5\lambda_0 \times 5\lambda_0 \times 2.5\lambda_0$ at the microwave carrier frequency $f_0 = 2.45$ GHz. The microwave devices controlling the signal waveform allow for manipulation of high power microwave signals with a maximum bandwidth of 250 MHz around the carrier frequency, *i.e.* a minimum pulse duration of 8 ns [18]. The cavity also includes a faradized window to observe the plasma discharges and several electrical feedthroughs for transferring the microwave signals.

Three small coaxial probes acting as monopoles are thus inserted into the cavity. In Fig. 1, these monopoles are colored in black, red and blue. The terminal of the black monopole, represented by $\mathbf{r}_0$, represents the source and is used in the second step of the TR or the LCCF experiments. It is located in an appendix of the cavity at atmospheric pressure to prevent gas breakdown in its vicinity during the emission of a high power signal. This appendix is connected to the main cavity through a glass window. The two other red and blue monopoles, numbered 1 and 2, are located in the main cavity filled with argon at a working pressure of 133 Pa. We respectively represent by $\mathbf{r}_p$ and $\mathbf{r}_z$ the terminals of monopoles 1 and 2, and further we assume that the aim is to generate plasma at $\mathbf{r}_p$ and prevent parasitic discharge at $\mathbf{r}_z$. The monopole $\mathbf{r}_p$ is used as a probe for the first phase of the TR to record the experimental impulse response with $\mathbf{r}_0$ (as opposed to "impulse response" which refers by definition to the response of a system to a Dirac excitation). The monopole $\mathbf{r}_z$, for example in the case presented in Fig. 1, is here to model an irregularity inside the cavity. However, for the LCCF method, both $\mathbf{r}_p$ and $\mathbf{r}_z$ are simultaneously used as probes to record their impulse responses with $\mathbf{r}_0$.

In our experiments, $\mathbf{r}_z$ is chosen with a sharp tip to represent an irregularity while used to monitor the temporal field evolution at its position during our experiments. During a TR experiment at $\mathbf{r}_p$, parasitic discharges are obtained near the metallic tip of $\mathbf{r}_z$, as illustrated in Fig. 1(a). Note that, the use of electro-optic probes would make it possible to obtain the various experimental impulse responses in a non-intrusive manner in a more realistic system.

III. PLASMA CONTROL BY THE TR METHOD

The spatial control of microwave plasmas using TR has already been presented by Mazières *et al.* [18]. At first the experimental impulse response between $\mathbf{r}_p$ and $\mathbf{r}_0$ is recorded and time reversed. Then, this signal is amplified using a 2 kW traveling wave tube pulsed power amplifier (TMD PTC7353) with a repetition period of $T_{ampli} = 16.6$ μs, and transmitted to the cavity by $\mathbf{r}_0$. It finally generates a spatio-temporal focusing of the electromagnetic energy at $\mathbf{r}_p$. If the level of these microwave signals is high enough, plasma breakdown may appear near $\mathbf{r}_p$. Thus, using the TR technique, the position $\mathbf{r}_p$ of the plasma can be controlled only by manipulating the signal waveform [18].

TR is very effective for controlling the position of the microwave plasmas inside the cavity. However, when increasing the power injected, TR inevitably leads to an increase in the electric field magnitude elsewhere in the cavity. This field may be high enough to reach plasma breakdown condition, especially near an irregularity. The same events occur in our cavity: During the TR experiment at $\mathbf{r}_p$ with a high level of the refocused peak, a plasma breakdown is obtained. Meanwhile, as expected, parasitic discharges appear at $\mathbf{r}_z$. The TR experiment is illustrated in Fig. 1(a) and reported in Fig. 2(a).

Such parasitic discharges can be avoided by advanced transient electric field shaping methods, which cancel or at least reduce the electric field at their location during the whole experiment. An effective way is to use the LCCF method, as we show in the next section.

IV. PLASMA CONTROL BY THE LCCF METHOD

A. THE LCCF METHOD

In the problem to be solved, we first represent the cavity as a three dimensional domain denoted by Ω. The propagation of the waves inside Ω are described through the evolution of the electric field $\mathbf{E} = \mathbf{E}(\mathbf{r},t)$ and the magnetic field $\mathbf{H} = \mathbf{H}(\mathbf{r},t)$ where $(\mathbf{r},t) \in \Omega \times [0,t_n] \subseteq \mathbb{R}^3 \times \mathbb{R}_+^*$. The instant $t_n = n\Delta t$ $(n \in \mathbb{N}^*)$ is the last instant of time to be specified and Δt represents the time step of discretization. At an instant t, a monopole, placed at a fixed position $\mathbf{r}_0$ of the cavity, excites Ω through a current density source $\mathbf{J} = \mathbf{J}(\mathbf{r}_0,t)$. The propagation of $\mathbf{E}$ and $\mathbf{H}$ are described by time-dependent Maxwell's equations of the following form

$$\varepsilon \frac{\partial \mathbf{E}}{\partial t} = \nabla \times \mathbf{H} - \sigma \mathbf{E} - \mathbf{J} \tag{1}$$

$$\mu \frac{\partial \mathbf{H}}{\partial t} = -\nabla \times \mathbf{E} \tag{2}$$

where $\varepsilon = \varepsilon(\mathbf{r})$, $\mu = \mu(\mathbf{r})$, and $\sigma = \sigma(\mathbf{r})$ are the local permittivity, permeability, and conductivity of Ω, respectively. The boundary conditions are defined by the cavity walls, but, in general, arbitrary boundary conditions may be added to the problem. The aim of the LCCF method is to identify a temporal current density source $\mathbf{J}$ (or more) in order to control $\mathbf{E}$ and $\mathbf{H}$ at $N \in \mathbb{N}^*$ spatial

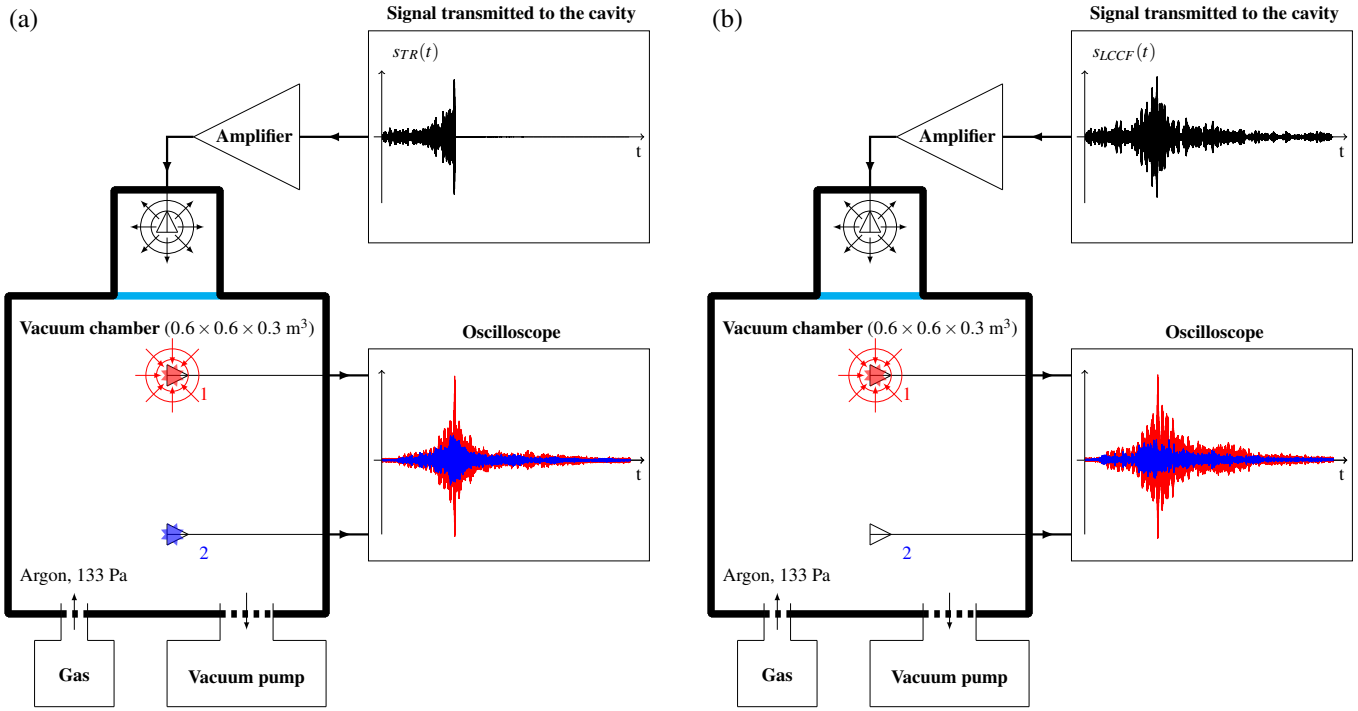

Figure 1. (a) Sketch of the TR experiment at monopole 1. The time reversed experimental impulse response between the red monopole 1 and the black monopole in the appendix $s_{TR}(t)$ is used to obtain a 8 ns peak at monopole 1. In this experiment, the level of the signal transmitted to the cavity is high enough to obtain plasma breakdown near monopole 1. Unfortunately, parasitic discharges are simultaneously generated near the blue monopole 2. This occurs as the microwave level at monopole 2 is high enough to reach the microwave plasma breakdown threshold. (b) Sketch of the LCCF experiment. The target signal at monopole 1 corresponds to the signal measured at the same monopole during the TR experiment. However, the target signal at monopole 2 is set to zero. As required in this case, the peak obtained at monopole 1 is similar to that obtained by the TR experiment. Interestingly, the signal level at monopole 2 is reduced when compared to the signal obtained at the same monopole during the TR experiment.

positions $\mathbf{r}_1, \cdots, \mathbf{r}_N$ of Ω over a predefined time interval. This time interval is called the "target time" and denoted by $[t_q, t_f] = [q\Delta t, f\Delta t] \subseteq [0, t_n] : (q, f) \in \mathbb{N}^2$ representing the duration throughout which we are interested in controlling $\mathbf{E}$ and $\mathbf{H}$. In a previous work, the authors developed a numerical procedure, named the LCCF method [41], to find a current density source that leads to a desired target electric field at several spatial points over a target time.

Without loss of generality, the LCCF method may be used to control any electric (E_x, E_y, E_z) or magnetic (H_x, H_y, H_z) components. In our experiment, only one component of the electric field is measured by each monopole in the cavity, then the LCCF method is presented to control the E_x component of the electric field, for instance, which is colinear with the monopole. To adapt the LCCF method to the spatial control of plasmas, we use the generalized version of the LCCF method [43] to identify the temporal profile of a single current density source $J_x(t)$ that imposes distinct target electric fields $E_x^1(t)$ and $E_x^2(t)$ at two positions $\mathbf{r}_1$ and $\mathbf{r}_2$, respectively, for $t \in [t_q, t_f]$. The positions $\mathbf{r}_1$ and $\mathbf{r}_2$ correspond to the two monopoles placed at the measuring points in the cavity. The LCCF method is based on solving the following linear system

$$\begin{pmatrix} \mathbf{A}_1 \\ \mathbf{A}_2 \end{pmatrix} \mathbf{J}_x = \begin{pmatrix} \mathbf{E}_x^1 \\ \mathbf{E}_x^2 \end{pmatrix}, \tag{3}$$

where $\mathbf{J}_x = \left[J_x(t_0), J_x(t_1), \ldots, J_x(t_f)\right]$ stands for the discretized current density source and similarly for $\mathbf{E}_x^1$ and $\mathbf{E}_x^1$. For the sake of clarity, we use the notation $\mathbf{A} = \begin{pmatrix} \mathbf{A}_1 \\ \mathbf{A}_2 \end{pmatrix}$ and $\mathbf{E}_x^{1,2} = \begin{pmatrix} \mathbf{E}_x^1 \\ \mathbf{E}_x^2 \end{pmatrix}$ in the rest of the paper. For $i \in \{1, 2\}$ we have

- $\mathbf{J}_x \in \mathbb{R}^{f+1}$ as the discrete source computed by the LCCF method to control the x-component of the electric field over the target time $[t_q, t_f]$;
- $\mathbf{E}_x^i \in \mathbb{R}^{f-q+1}$ as the discrete target field to be obtained at $\mathbf{r}_i$ over $[t_q, t_f]$ after emitting the source;
- $\mathbf{A}_i \in \mathbb{M}_{(f-q+1)\times(f+1)}$ as the LCCF transfer matrix to characterize the system between the source point $\mathbf{r}_0$ and $\mathbf{r}_i$ during $[t_q, t_f]$. For more details on how to construct $\mathbf{A}_i$ the reader may refer to Benoit *et al.* [41].

System (3) is not square and may be solved for $\mathbf{J}_x$ in the least square sense by premultiplying both sides by $\mathbf{A}^T$. The singular matrix $\mathbf{A}^T\mathbf{A}$ is ill-conditioned, so its inversion $\left(\mathbf{A}^T\mathbf{A}\right)^{-1}$ is numerically unstable. For this reason, we use Tikhonov regularization [44] to stabilize the LCCF system as follows

$$\left(\mathbf{A}^T\mathbf{A} + \varepsilon\mathbf{I}\right)\mathbf{J}_x = \mathbf{A}^T\mathbf{E}_x^{1,2}, \tag{4}$$

where $\mathbf{I}$ is the identity matrix of size $f+1$. The Tikhonov parameter $\varepsilon > 0$ is heuristically chosen to be small enough

so as not to distort the solution. In this paper, we take $\varepsilon = 10^{-9}$.

Recently, it was shown that matrix $\mathbf{A}_i$ is built relying only on the impulse response of the system between the source point and $\mathbf{r}_i$ [42]. That is to say, we emit a unit impulse $\delta = (1,0,\cdots,0)$ and record the response $\mathbf{h}_\delta$ obtained at $\mathbf{r}_i$. As we propose, in this paper, to experimentally apply the LCCF technique in 3D, the impulse response computed to create the matrix $\mathbf{A}_i$ may be theoretically and numerically realizable, but not experimentally due to the impossible emission of δ. As an alternative solution, $\mathbf{A}_i$ is built by considering the response of any incident pulse denoted by $\alpha = [\alpha(0),\alpha(1),\cdots,\alpha(n)] \neq \delta$ that may be realized experimentally. Let $\tilde{\mathbf{A}}_i$ be the LCCF matrix constructed in exactly the same way as $\mathbf{A}_i$, but this time based on the response of α and not the impulse response of δ. If we denote by $\mathbf{h}_\alpha$ the response of α at $\mathbf{r}_i$, $\tilde{\mathbf{A}}_i$ may explicitly be written as

$$\tilde{\mathbf{A}}_i = \begin{pmatrix} h_\alpha(q) & h_\alpha(q-1) & \cdots & h_\alpha(0) & & \\ \vdots & h_\alpha(q) & \ddots & \ddots & \ddots & \mathbf{0} \\ \vdots & \vdots & \ddots & \ddots & \ddots & \\ h_\alpha(f) & h_\alpha(f-1) & \cdots & \cdots & \cdots & h_\alpha(0) \end{pmatrix}. \tag{5}$$

Using the new notation, the LCCF system becomes after regularization

$$\left(\tilde{\mathbf{A}}^T\tilde{\mathbf{A}} + \varepsilon\mathbf{I}\right)\widetilde{\mathbf{J}}_x = \tilde{\mathbf{A}}^T\mathbf{E}_x^{1,2} \tag{6}$$

By solving system (6), $\widetilde{\mathbf{J}}_x$ is computed. In fact, the source $\widetilde{\mathbf{J}}_x$ is the expression of $\mathbf{J}_x$ computed in another basis. Injecting $\widetilde{\mathbf{J}}_x$ at $\mathbf{r}_0$ does not produce the target signals $\mathbf{E}_x^i$ at $\mathbf{r}_i$ since $\tilde{\mathbf{A}}$ does not represent the characterization matrix of the system. This is why it is necessary to compute $\mathbf{J}_x$ through $\widetilde{\mathbf{J}}_x$ using basic concepts of linear algebra. For all $k \in \{0,\cdots,f\}$, let $\alpha_k = [\mathbf{0}_k, \alpha(0),\cdots,\alpha(f-k)]$ where $\mathbf{0}_k$ is the zero vector of length k. Denote by $\mathscr{C} = \{\mathbf{e}_0,\cdots,\mathbf{e}_f\}$ the canonical basis of the $(f+1)$-dimensional vector space $\mathbb{R}^{f+1}$. Assuming that $\mathscr{B} = \{\alpha_0,\cdots,\alpha_f\}$ also forms a basis of $\mathbb{R}^{f+1}$, then there exists an invertible matrix $\mathbf{P}$ called the transition matrix from $\mathscr{C}$ to $\mathscr{B}$ such that

$$\alpha_k = \mathbf{P}\mathbf{e}_k,\ k \in \{0,\cdots,f\}, \tag{7}$$

and $\mathbf{J}_x$ and $\widetilde{\mathbf{J}}_x$ are linked by the relation

$$\mathbf{J}_x = \mathbf{P}\widetilde{\mathbf{J}}_x. \tag{8}$$

In the rest of the paper, $\mathbf{r}_1$ (resp. $\mathbf{r}_2$) represents $\mathbf{r}_p$ (resp. $\mathbf{r}_z$) and $\mathbf{E}_x^1$ (resp. $\mathbf{E}_x^2$) represents the electric target signal to be produced at $\mathbf{r}_p$ (resp. $\mathbf{r}_z$) denoted henceforth by $\mathbf{E}_x^p$ (resp. $\mathbf{E}_x^z$). Furthermore, α is chosen to be a Sine-Gaussian signal to construct the LCCF matrices $\tilde{\mathbf{A}}_p$ and $\tilde{\mathbf{A}}_z$, however any other physically achievable signal could similarly be considered. Since we aim at generating plasma at $\mathbf{r}_p$ and preventing parasitic discharges at $\mathbf{r}_z$, then the last instant of the target time t_f is the instant just after the period at which plasma is generated at $\mathbf{r}_p$, while for $\mathbf{r}_z$, $t_f = t_n$ as we wish to avoid generating parasitic discharges for the entire time interval.

B. THE LCCF METHOD FOR PLASMA CONTROL

1) Principle

In our experimental setup, the electric field behavior inside the cavity can be controlled (or monitored) through the voltage signals applied (or measured) at the terminals of the monopoles. Since a linear relation exists between the voltage source and the electromagnetic fields in the cavity, in practice, the LCCF method computes a temporal source $\mathbf{J}_x$. For the sake of clarity, we will use the notation $\mathbf{s}_{LCCF} = \left[s_{LCCF}(t_0),\ldots,s_{LCCF}(t_f)\right]$ instead of $\mathbf{J}_x$. The latter, transmitted to the cavity through a source point, makes it possible to impose one (or several) chosen target signal(s) at one (or several) target point(s) inside the cavity. Thus, the behavior of waves can be controlled at one or several chosen locations inside the cavity during a long duration, unlike the original TR method where the behavior of waves can be controlled during the pulse duration only.

The target signals $\mathbf{E}_x^p$ and $\mathbf{E}_x^z$ may theoretically hold any shape as long as they are physically achievable. For our plasma experiments, we want the lowest possible electromagnetic level at $\mathbf{r}_z$ (so that no parasitic discharges are observed) and a peak with the highest possible level at $\mathbf{r}_p$ (so that a plasma is generated during the peak). Ideally, a zero signal is desired at $\mathbf{r}_z$ for the entire time interval, *i.e.*, $\mathbf{E}_x^z = \mathbf{0}$. Similarly, for $\mathbf{r}_p$, a zero signal is desired as well, except for a certain time duration where a high focusing peak is imposed, *i.e.*, $\mathbf{E}_x^p = [0,\ldots,0,a_1,\ldots,a_m,0,\ldots,0]$ where $a_1,\ldots,a_m \gg 0$. It is easily conceivable that this configuration is not realizable in practice, at least in our experimental conditions, as it would come up against some physical limitations.

For our application, focusing of the waves is crucial to obtaining a localized electric field high enough in order to generate plasma at $\mathbf{r}_p$. Apprehending the spatial focusing of the waves on the shape of the signals measured in the time domain is complicated, if not impossible. Indeed, it would be difficult to create a target signal from scratch in which one peak corresponds to spatial focusing of the waves. The idea developed in this paper is to start from the TR signal (measured at $\mathbf{r}_p$) as the target signal. This leads to simultaneous manipulation of the target signals to suit focusing of the waves and fit the physical constraints of the experiment. Based on this idea, we use the LCCF method to synchronously produce a signal with a focusing peak at $\mathbf{r}_p$ and a signal with the lowest possible level at $\mathbf{r}_z$.

The LCCF method is then used for plasma control as follows: To obtain plasma at $\mathbf{r}_p$, the corresponding target signal $\mathbf{E}_x^p$ is taken equal to the signal obtained during the TR experiment at $\mathbf{r}_p$, and a target signal $\mathbf{E}_x^z$ equal to zero is imposed at $\mathbf{r}_z$. It is clear that, as the waves propagate inside the cavity, they will often encounter the monopole $\mathbf{r}_z$, so it would certainly be physically impossible to obtain a zero signal during the whole process. However the LCCF

method will give a configuration close to the ideal zero signal in the least square sense, as long as it is physically realizable. The aim is to obtain the refocused peak at $\mathbf{r}_p$ so that plasma breakdown occurs as it does for the TR. Besides generating the peak at $\mathbf{r}_p$, the advantage of the LCCF method over the TR is its ability to synchronously reduce the signal magnitude at $\mathbf{r}_z$ for the entire time interval. As a result, parasitic discharges are avoided at $\mathbf{r}_z$ during the whole experimental process. For that, we rely on the linear least squares solver to compute $\mathbf{s}_{LCCF}$ which minimizes the quantity $\left\| \left(\mathbf{A}^T\mathbf{A} + \varepsilon\mathbf{I}\right)\mathbf{s}_{LCCF} - \mathbf{A}^T\mathbf{E}_x^{p,z} \right\|_2^2$.

2) Results

By following the method described in the previous paragraph the LCCF method succeeds in reconstructing the focusing peak at $\mathbf{r}_p$ with the same level as that obtained by TR (see the red signals in Fig. 1). As for the TR experiment, the microwave power contained in this peak is high enough to reach plasma breakdown condition near $\mathbf{r}_p$. Plasma discharge is then observed at $\mathbf{r}_p$, as shown in the images of Fig. 2(a).

The measured signal at $\mathbf{r}_z$ is shown in the first two subfigures of Fig. 2(a) during the TR and the LCCF experiments. The level obtained at $\mathbf{r}_z$ during the LCCF experiment is lower than with the TR experiment. However, the observed signal is far from the identically zero signal. To understand the origin of this difference, it is useful to look at this signal in the frequency domain, as represented in the second two subfigures of Fig. 2(a). Only the useful bandwidth is plotted, lying between 500 MHz around the carrier frequency $f_0 = 2.45$ GHz. First we can notice the multimodal property of the cavity on this bandwidth. This property is essential for our TR or LCCF experiments to work. We see here the difficulty the LCCF method encounters when a zero signal is desired. The impossibility to impose a zero signal (with the same experimental setup and conditions) is due to the many modes that are excited during the experiment. However, the LCCF method manages to find a solution in which the influence of the mode with the highest amplitude, namely around 2.5 GHz here, is considerably reduced. In Fig. 2(b), we switch the notation $\mathbf{r}_p$ and $\mathbf{r}_z$. We denote now by $\mathbf{r}_p$ the terminal of blue monopole 2 and by $\mathbf{r}_z$ the terminal of red monopole 1, *i.e.* we carry out the same experiment, but the objective here is to generate plasma at monopole 2 and avoid discharges at monopole 1. Similar to what came before, the same analysis may be conducted, and we clearly observe that the LCCF efficiently generates plasma at $\mathbf{r}_p$ and prevents parasitic discharges at $\mathbf{r}_z$.

The images in Fig. 2 clearly show that the plasma location is well controlled during the LCCF experiment, whereas parasitic plasmas are generated during the TR experiment. Interestingly, we may note that plasma breakdown is a threshold phenomenon. After emitting the LCCF source, although the level of the signal measured at $\mathbf{r}_z$ is not identically zero, its level is quite low *i.e.* below plasma

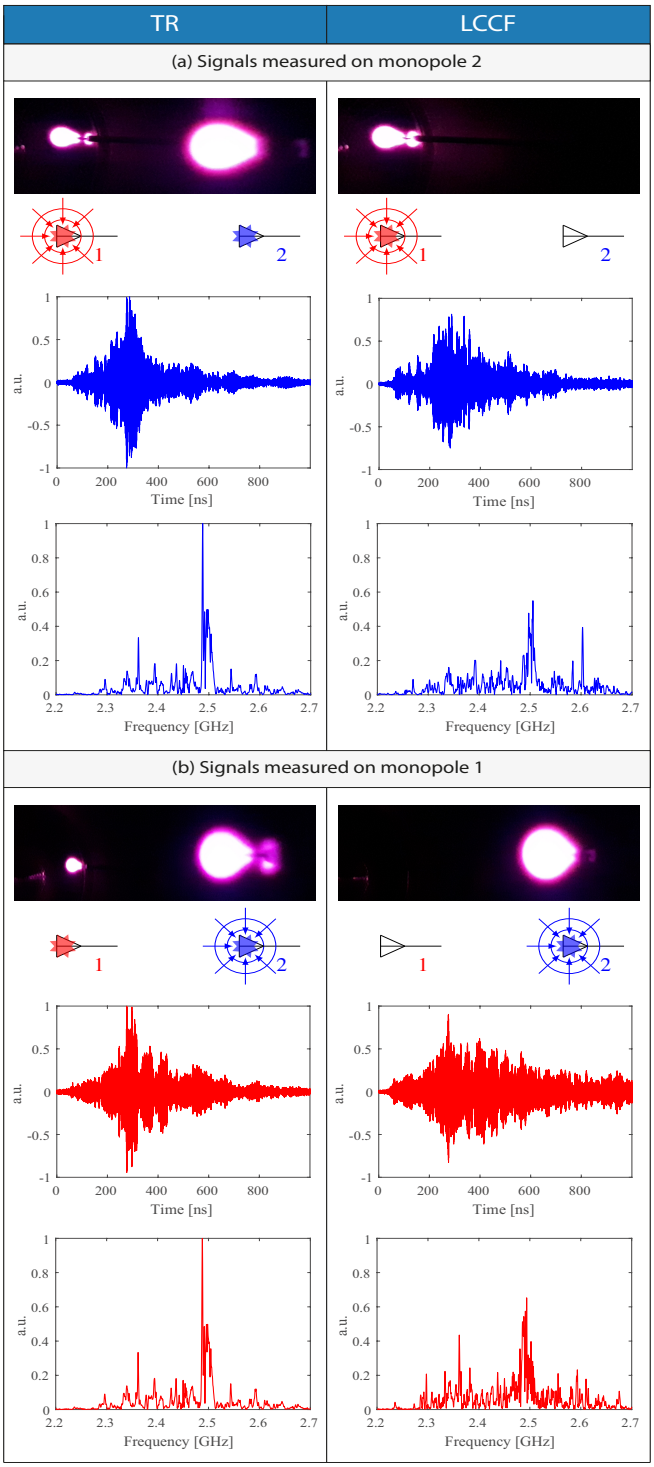

Figure 2. Results of the TR and the LCCF experiments. (a) During the TR experiment, we successfully generate plasma at monopole 1; however, parasitic discharges appear at monopole 2. Alternatively, the LCCF is used to generate plasma only at monopole 1. The four subfigures represent the electric field obtained at monopole 2 during the TR and the LCCF experiments in the frequency and time domain. (b) The same TR and LCCF experiments of (a) are repeated but this time the aim is to generate plasma at monopole 2 and prevent discharges at monopole 1. The four subfigures represent the electric field obtained at monopole 1 during the TR and the LCCF experiments in the frequency and time domain.

breakdown condition.

Finally, during the LCCF experiment, the level at $\mathbf{r}_z$ is lowered, preventing the formation of parasitic discharges at this position. In contrast, during the TR experiment with the same level of refocused peak, a plasma was generated at $\mathbf{r}_z$, as shown in Figure 2. The LCCF allows to deposit high power in the plasma near $\mathbf{r}_p$ without any parasitic discharge, whereas it is not possible by TR with the same experimental setup in the same conditions.

V. CONCLUSION

We experimentally investigated the capabilities of the linear combination of configuration field method to generate and control nanosecond microwave plasmas in an all-metal plasma reactor. It has been shown that the LCCF method prevents parasitic discharges by controlling the electric field at several locations in the plasma reactor, and this during the spatio-temporal focusing operation. The microwave control capabilities of the LCCF method makes it a good candidate for the sophistication of the recently developed plasma source [18]. This 3D transient electric field shaping method clearly pushes back the capabilities of this source as a promising microwave "plasma brush".

In this paper, the duration of the plasma is very short, and it is generated only at a single spatial point. This will not be the case for the "plasma brush" and the nonlinear effects can no longer be neglected. A recent work has been published about controlling electromagnetic fields in nonlinear systems [45] that seems to be promising for enhanced spatial control of microwave plasmas in a nonlinear cavity.

References

[1] C. M. Ferreira and M. Moisan, Eds., Microwave Discharges: Fundamentals and Applications. Springer US, 1993.

[2] A. Grill, Cold Plasma in Materials Fabrication: From Fundamentals to Applications. Wiley-IEEE Press, 1994.

[3] M. A. Lieberman and A. J. Lichtenberg, Principles of Plasma Discharges and Materials Processing. John Wiley & Sons, 2005.

[4] T. Lagarde, J. Pelletier, and Y. Arnal, "Influence of the multipolar magnetic field configuration on the density of distributed electron cyclotron resonance plasmas," Plasma Sources Sci. Technol., vol. 6, no. 1, pp. 53–60, Feb. 1997.

[5] Y. A. Lebedev, "Microwave discharges at low pressures and peculiarities of the processes in strongly non-uniform plasma," Plasma Sources Sci. Technol., vol. 24, no. 5, p. 053001, Aug. 2015.

[6] H. Schlüter and A. Shivarova, "Travelling-wave-sustained discharges," Phys. Rep., vol. 443, no. 4, pp. 121–255, May 2007.

[7] M. Moisan, Z. Zakrzewski, and R. Pantel, "The theory and characteristics of an efficient surface wave launcher (surfatron) producing long plasma columns," J. Phys. D: Appl. Phys., vol. 12, no. 2, pp. 219–237, Feb. 1979.

[8] M. Moisan, Z. Zakrzewski, R. Pantel, and P. Leprince, "A waveguide-based launcher to sustain long plasma columns through the propagation of an electromagnetic surface wave," IEEE Trans. Plasma Sci., vol. 12, no. 3, pp. 203–214, Sep. 1984.

[9] H. Tahara, J. Kitayama, T. Yasui, K. Onoei, Y. Tsubakishita, and T. Yoshikawa, "Long plasma generation using microwave slot antennas on a rectangular waveguide," Rev. Sci. Instrum., vol. 65, no. 3, pp. 669–672, Mar. 1994.

[10] F. Werner, D. Korzec, and J. Engemann, "Slot antenna 2.45 GHz microwave plasma source," Plasma Sources Sci. Technol., vol. 3, no. 4, pp. 473–481, Nov. 1994.

[11] F. C. Fehsenfeld, K. M. Evenson, and H. P. Broida, "Microwave discharge cavities operating at 2450 MHz," Rev. Sci. Instrum., vol. 36, no. 3, pp. 294–298, Mar. 1965.

[12] J. Asmussen, R. Mallavarpu, J. R. Hamann, and H. C. Park, "The design of a microwave plasma cavity," Proc. IEEE, vol. 62, no. 1, pp. 109–117, Jan. 1974.

[13] F. Silva, K. Hassouni, X. Bonnin, and A. Gicquel, "Microwave engineering of plasma-assisted CVD reactors for diamond deposition," J. Phys.: Condens. Matter, vol. 21, no. 36, p. 364202, Aug. 2009.

[14] B. Dischler and C. Wild, Eds., Low-Pressure Synthetic Diamond: Manufacturing and Applications. Springer-Verlag, 1998.

[15] Y. F. Li, J. J. Su, Y. Q. Liu, M. H. Ding, X. L. Li, G. Wang, P. L. Yao, and W. Z. Tang, "Design of a new TM021 mode cavity type MPCVD reactor for diamond film deposition," Diamond Relat. Mater., vol. 44, pp. 88–94, Apr. 2014.

[16] M. Füner, C. Wild, and P. Koidl, "Novel microwave plasma reactor for diamond synthesis," Appl. Phys. Lett., vol. 72, no. 10, pp. 1149–1151, Mar. 1998.

[17] J. J. Su, Y. F. Li, X. L. Li, P. L. Yao, Y. Q. Liu, M. H. Ding, and W. Z. Tang, "A novel microwave plasma reactor with a unique structure for chemical vapor deposition of diamond films," Diamond Relat. Mater., vol. 42, pp. 28–32, Feb. 2014.

[18] V. Mazières, R. Pascaud, L. Liard, S. Dap, R. Clergereaux, and O. Pascal, "Plasma generation using time reversal of microwaves," Appl. Phys. Lett., vol. 115, no. 15, p. 154101, Oct. 2019.

[19] G. Lerosey, J. de Rosny, A. Tourin, A. Derode, G. Montaldo, and M. Fink, "Time reversal of electromagnetic waves," Phys. Rev. Lett., vol. 92, p. 193904, May 2004.

[20] A. Khaleghi, "Measurement and analysis of ultra-wideband time reversal for indoor propagation channels," Wireless Pers. Commun., vol. 54, pp. 307–320, Jul. 2010.

[21] W. Lei and L. Yao, "Performance analysis of time reversal communication systems," IEEE Commun. Lett., vol. 23, no. 4, pp. 680–683, Apr. 2019.

[22] F. Foroozan and A. Asif, "Time reversal based active array source localization," IEEE Trans. Signal Process., vol. 59, no. 6, pp. 2655–2668, Jun. 2011.

[23] R. Ibrahim, D. Voyer, A. Bréard, J. Huillery, C. Vollaire, B. Allard, and Y. Zaatar, "Experiments of time-reversed pulse waves for wireless power transmission in an indoor environment," IEEE Trans. Microw. Theory Techn., vol. 64, no. 7, pp. 2159–2170, Jul. 2016.

[24] B. Li, S. Liu, H. Zhang, B. Hu, D. Zhao, and Y. Huang, "Wireless power transfer based on microwaves and time reversal for indoor environments," IEEE Access, vol. 7, pp. 114 897–114 908, 2019.

[25] G. Lerosey, J. de Rosny, A. Tourin, A. Derode, and M. Fink, "Time reversal of wideband microwaves," Appl. Phys. Lett., vol. 88, no. 15, p. 154101, 2006.

[26] C. Draeger and M. Fink, "One-channel time reversal of elastic waves in a chaotic 2D-silicon cavity," Phys. Rev. Lett., vol. 79, no. 3, pp. 407–410, Jul. 1997.

[27] U. Jordan, D. S. Dorozhkina, V. E. Semenov, T. Olsson, D. Anderson, M. Lisak, J. Puech, I. M. Nefedov, and I. A. Shereshevskii, "Microwave corona breakdown around metal corners and wedges," IEEE Trans. Plasma Sci., vol. 35, no. 3, pp. 542–550, Jun. 2007.

[28] P. M. Platzman and E. H. Solt, "Microwave breakdown of air in nonuniform electric fields," Phys. Rev., vol. 119, no. 4, pp. 1143–1149, Aug. 1960.

[29] J. Rasch, D. Anderson, M. Lisak, V. E. Semenov, and J. Puech, "Gas breakdown in inhomogeneous microwave electric fields," J. Phys. D: Appl. Phys., vol. 42, no. 20, p. 205203, Sep. 2009.

[30] F. Monsef and A. Cozza, "Average number of significant modes excited in a mode-stirred reverberation chamber," IEEE Trans. Electromagn. Compat., vol. 56, no. 2, pp. 259–265, Apr. 2014.

[31] A. Cozza and F. Monsef, "Multiple-source time-reversal transmissions in random media," IEEE Trans. Antennas Propag., vol. 62, no. 8, pp. 4269–4281, Aug. 2014.

[32] K. Selemani, J.-B. Gros, E. Richalot, O. Legrand, O. Picon, and F. Mortessagne, "Comparison of reverberation chamber shapes inspired from chaotic cavities," IEEE Trans. Electromagn. Compat., vol. 57, no. 1, pp. 3–11, Feb. 2015.

[33] A. Cozza, "Emulating an anechoic environment in a wave-diffusive medium through an extended time-reversal approach," IEEE Trans. Antennas Propag., vol. 60, no. 8, pp. 3838–3852, Aug. 2012.

[34] D. Zhao and M. Zhu, "Generating microwave spatial fields with arbitrary patterns," IEEE Antennas Wireless Propag. Lett., vol. 15, pp. 1739–1742, 2016.
[35] B. Li, D. Zhao, S. Liu, B.-J. Hu, and Y. Huang, "Precise transient electric field shaping with prescribed amplitude pattern by discrete time reversal," IEEE Access, vol. 7, pp. 84 558–84 564, 2019.
[36] R. Wang, J. Liu, Y. Lv, Z. Wang, S. Liu, M. Zhang, S. Ding, and B.-Z. Wang, "Subwavelength field shaping approach based on time reversal technique and defective metasurfaces," IEEE Access, vol. 7, pp. 84 629–84 636, 2019.
[37] A. G. Cepni and D. D. Stancil, "Single antenna microwave nulling using time-reversal techniques," in 2005 IEEE MTT-S Int. Microwave Symp. Digest, vol. 4, Jun. 2005, pp. 1723–1726.
[38] J. R. Punnoose, N. Jacklin, and D. Counsil, "Spatially focusing a radio signal and simultaneously nulling it at another location using time-reversal signal processing," in MILCOM 2011, Nov. 2011, pp. 401–405.
[39] M. Spirlet, "Correction of electromagnetic measurements and active shaping of electromagnetic fields in complex and reverberating environments," Ph.D. dissertation, Mar. 2018.
[40] M. Spirlet, C. Geuzaine, and V. Beauvois, "Optimal control theory applied to unintended source control and field shaping for time-harmonic electromagnetic waves," IEEE Transactions on Electromagnetic Compatibility, vol. 62, no. 1, pp. 65–73, Feb. 2020.
[41] J. Benoit, C. Chauvière, and P. Bonnet, "Source identification in time domain electromagnetics," J. Comput. Phys., vol. 231, no. 8, pp. 3446–3456, Apr. 2012.
[42] J. Benoit, C. Chauvière, and P. Bonnet, "Time-dependent current source identification for numerical simulations of maxwell's equations," J. Comput. Phys., vol. 289, pp. 116–128, May 2015.
[43] A. Al Ibrahim, C. Chauvière, and P. Bonnet, "Active electromagnetic interference control in time domain: application to software correction of defective lossy transmission-line networks," IEEE Trans. Electromagn. Compat., vol. 62, no. 2, pp. 355–363, Apr. 2020.
[44] A. N. Tikhonov, "Solution of incorrectly formulated problems and the regularization method," Soviet Math. Dokl., Jan. 1963.
[45] A. Al Ibrahim, C. Chauvière, and P. Bonnet, "Time-domain software correction of nonlinear faulty lossy transmission line networks," IEEE Transactions on Electromagnetic Compatibility, pp. 1–8, 2020.